International Journal of Heat and Technology
Vol. 41, No. 4, August, 2023, pp. 869-882
Journal homepage: http://iieta.org/journals/ijht

Thermal Conductivity and Shear Strength in Root-Reinforced Silty Clay: An Analysis of Asteraceae Plants from Taihang Mountain

Bingyu Wang[1,2], Shijie Wang[1*]

[1] Department of Civil Engineering, Hebei Agricultural University, Baoding 071001, China
[2] Hebei Provincial Institute of Building Science Co., Ltd, Hebei Provincial Construction Engineering Quality Inspection Center Co., Ltd, Shijiazhuang 050200, China

Corresponding Author Email: wshj_wshj@hebau.edu.cn

https://doi.org/10.18280/ijht.410409

Received: 4 May 2023
Revised: 20 July 2023
Accepted: 26 July 2023
Available online: 31 August 2023

Keywords:
silty clay, root reinforcement, thermal conductivity, thermal stress, temperature-seepage-stress coupling, shear strength

ABSTRACT

Silty clay, pivotal in domains spanning civil and environmental engineering to underground energy storage, demands precise characterisation of its thermal conductivity and shear strength. Root reinforcement has recently been heralded for its eco-friendly attributes and efficacy in enhancing soil properties. Nonetheless, extant literature remains focused on individual soil types, often sidelining the biological influence of entities like roots. Moreover, a reliance on experimental measurements in prior studies has precluded exhaustive theoretical discourse. Addressing these lacunae, the present investigation was embarked upon. Two focal areas emerged: firstly, an intricate exploration, underpinned by both experimental and simulated data, of the correlation between pore attributes and thermal conductivity in root-reinforced silty clay, and the concomitant repercussions on shear strength. Secondly, an encompassing appraisal of the thermal stress within this reinforced clay was conducted via a temperature-seepage-stress coupling model. Marigold root-soil composites became the central subjects, with an aim to discern the influence of herbaceous Asteraceae plants endemic to Taihang Mountain on parameters such as erosion resistance, soil consolidation, and shear resistance augmentation of soil masses. By harnessing raw soil samples, fashioning test specimens, and executing controlled triaxial compression experiments, intricate patterns pertaining to erosion resistance and soil consolidation, modulated by varying factors like root content, soil depth, and moisture content, were elucidated. The revelations herein promise to refine predictions of thermal conductivity and deepen the comprehension of shear strength dynamics in multifaceted soil scenarios.

1. INTRODUCTION

Silty clay, a soil type characterised by low thermal conductivity and pronounced rheology, is extensively utilised in diverse sectors, encompassing civil and environmental engineering to underground energy storage [1,2]. Its favoured status in foundational constructs, subterranean tunnels, and soil barriers underscores its pivotal role [1,2]. However, the intricate internal structure and variegated pore distribution have rendered the accurate prediction of its thermal conductivity and thermal stress behaviour formidable [3-6].

As the drive for sustainable development and ecological conservation gains momentum, attention has been directed towards the root reinforcement technique. This method, which involves the integration of plant root systems into soil masses, enhances mechanical and thermophysical attributes, making its systematic investigation both theoretically and practically indispensable.

In diverse engineering pursuits, the precision in forecasting thermal conductivity and thermal stress stands paramount [7,8]. Major deviations from expected outcomes can either jeopardise projects or inflate associated expenditures. A nuanced understanding of the thermal attributes of root-reinforced silty clay augments the reliability and accuracy of engineering designs, offering pivotal insights for emerging geothermal energy systems, soil improvement, and ecological conservation [9-14]. Additionally, such research elucidates novel strategies for addressing thermal challenges in multifaceted soil environments, thereby propelling advancements in soil amelioration technology and environmental engineering.

Despite an abundance of studies on the thermal dynamics of silty clay, a discernible focus is evident: investigations predominantly target singular soil types, often overlooking the interplay of biology, particularly plant root systems [15-19]. Moreover, extant literature is replete with experiments, often sidelining methodical theoretical analyses [20-27]. For instance, a preponderance of studies have been noted to quantify thermal conductivity through mere experimental measurements, abstaining from dissecting influences like pore configurations, seepage conditions, or stress states. Such oversight precludes a holistic and precise depiction of the thermophysical attributes and thermal stress responses of root-reinforced silty clay across diverse operational and environmental settings.

Addressing these identified gaps, the core tenets of this investigation are bifurcated. Initially, both experimental and simulation techniques were harnessed to discern the nexus between pore attributes in root-reinforced silty clay and its thermal conductivity. In this endeavour, a gamut of

experiments was orchestrated, coupled with the formulation of a mathematical model grounded on acquired data to refine thermal conductivity predictions. Subsequently, a temperature-seepage-stress coupling model was employed, facilitated by state-of-the-art numerical analysis techniques, to probe the thermal stress dynamics within root-reinforced silty clay. Outcomes from these deliberations not only augment the accuracy and reliability of thermal conductivity predictions but also enrich comprehension of thermal stress generation and dispersion paradigms in intricate soil matrices. This study, thus, stands poised to contribute both to theoretical discourse and pragmatic implementations.

2. RELATIONSHIP BETWEEN PORE CHARACTERISTICS AND THERMAL CONDUCTIVITY OF ROOT-REINFORCED SILTY CLAY

Pore characteristics have a direct and significant influence on the thermal conductivity of soil. As for silty clay, due to its unique micro-structure and pore distribution, the prediction and analysis of its thermal conductivity is more complex, and the adding of root system may further increase this complexity since the root system can change the structure and distribution of pores in the soil. Thus, an in-depth analysis on the relationship between pore characteristics and thermal conductivity not only facilitates more accurate prediction of thermal conductivity, but also provides evidences for the optimization of root reinforcement techniques.

This paper begins with an analysis of the thermal conductivity of root-reinforced silty clay and its influencing factors, and the key in this stage is to figure out and quantify the factors that have the greatest influence on the thermal conductivity of root-reinforced silty clay. This may involve complex experimental designs that include multiple control variables such as the initial moisture content of soil, root density, and the mineral composition of soil, and the relative importance of these factors can be more accurately quantified through experiment or numerical simulation.

Assuming: z represents the direction of heat flow, η_z represents the thermal conductivity of heat flow in direction z, a represents the heat transfer area of heat flow on media surface, W represents the amount of heat transferred per unit area per unit time, w_z represents the density of heat flow in direction z, $\partial Y/\partial z$ represents the temperature gradient in direction z, then the heat transfer equation of the root-reinforced silty clay is:

$$\beta_W = -\eta da \frac{\partial Y}{\partial z} \tag{1}$$

$$\lambda_x = -\frac{\partial Q}{\partial s} \Big/ \frac{\partial T}{\partial x} = -q_x \Big/ \frac{\partial T}{\partial x} \tag{2}$$

Building empirical relational equations usually requires the support of large amounts of data, not just limited to the measurement of thermal conductivity under root-reinforced and non-root-reinforced conditions, the soil properties at multiple scales (such as porosity and moisture content at macro and micro levels) may be involved as well. Through data analysis, the interactions between these complex variables can be captured more accurately, based on which, the thermal conductivity can be predicted accordingly.

This paper chose to discuss the relationship between the dry density of root-reinforced silty clay and its thermal conductivity. Assuming: η represents the thermal conductivity of root-reinforced silty clay, q represents water content, ϑf represents dry density, then the empirical equation of thermal conductivity of root-reinforced silty clay is given by the following formula:

$$\eta = 0.15\left[0.95\lg q - 0.18\right] \times 10^{0.63\vartheta f} \tag{3}$$

Via experiment, it's known that there is a significant linear correlation between the dry density of the root-reinforced silty clay and the logarithm of its thermal conductivity, and the attained fitted linear equation is:

$$\lg \eta_0 = 0.36\vartheta f - 0.43 \tag{4}$$

The fractional dimension of particle distribution is a complex but highly informative parameter that describes the complexity of soil micro-structure. With the help of high-resolution imaging techniques and complex network analysis, this paper analyzed the relationship between particle distribution and thermal conductivity at multiple scales. This step may need to consider how particles and pores jointly affect the thermal conductivity, especially after the root system has been added.

This paper combined above equation with the relationship equation between dry density and the fractional dimension of particle distribution, then the following formula gives the relationship between the thermal conductivity of root-reinforced silty clay specimens and the fractional dimension of particle distribution:

$$\lg \eta_0 = 0.3584 \times \left(\frac{-1.993 \pm \sqrt{5.003 - 2.596F}}{-1.298} \right) - 0.4298 \tag{5}$$

The size, shape and distribution of pores can all affect the thermal conductivity, especially in root-reinforced soils, the root system may cause significant changes in pore structure. Therefore, this paper focuses on how to quantify these changes and their relationships with the thermal conductivity. Based on the fractal theory, this paper derived the fractal dimension of pore diameter distribution of root-reinforced silty clay, and the relationship between the thermal conductivity of root-reinforced silty clay and the fractal dimension of pore diameter distribution:

$$\lg \eta_0 = 0.3584 \times \frac{-37.355 \pm \sqrt{71.988 - 46.946F}}{-23.474} - 0.4298 \tag{6}$$

3. TEMPERATURE-SEEPAGE-STRESS COUPLING CALCULATIONS OF ROOT-REINFORCED SILTY CLAY

Silty clay is used in a variety of scenarios such as civil and environmental engineering, where the temperature, seepage, and stress of the soil are usually coupled with each other, and this coupling relationship has significant effects on the thermal stress behaviour of soil. However, existing studies haven't fully considered this coupling relationship, especially after the root system of plants has been added, significant changes can

happen to it, so studying the thermal stress behaviour of root-reinforced silty clay through calculating the coupling between temperature, seepage, and stress can help reveal the performance of this composite material under different working conditions.

Content of previous sections, the analysis of the relationship between pore characteristics and thermal conductivity of root-reinforced silty clay, and the temperature-seepage-stress coupling calculations together constituted a comprehensive framework of understanding. The analysis of pore characteristics and thermal conductivity provides basic data of physical properties and theoretical support for subsequent temperature-seepage-stress coupling calculations. In other words, accurate prediction of thermal conductivity will play a key role in the coupling calculation, especially in complex environments where temperature interacts with other physical processes such as seepage and stress. On the other hand, the calculation results of temperature-seepage-stress coupling can verify the accuracy and application scope of the pore characteristics-thermal conductivity relationship model, thereby further optimizing the design of the application of root-reinforced silty clay.

At first, the seepage-stress coupling was calculated in this paper. With pore structure and particle distribution taken into consideration, a representative porous medium model was established to describe the root-reinforced silty clay. Then, according to previous studies on thermal conductivity and pore characteristics, the necessary physical parameters were input, such as permeability and modulus of elasticity. At last, the finite element method and other appropriate numerical methods were employed in simulation to get the distribution characteristics of seepage and stress under different conditions.

Purpose of above steps is to figure out the behaviour of root-reinforced silty clay under the action of complex environmental factors, especially in case of seepage and stress. Specifically, a representative control volume was determined, including soil, water, and roots. Assuming: o represents the pore water pressure, L represents the biot modulus, γ represents the volumetric strain, β represents the biot coefficient, Y represents the temperature, by applying the principle of conservation of mass in the control volume, a mass conservation equation can be established for the saturated soil-water-root system:

$$\frac{\partial \delta}{\partial y} = \frac{1}{L}\frac{\partial o}{\partial y} + \beta \frac{\partial \gamma}{\partial t} - \alpha \frac{\partial Y}{\partial y} \tag{7}$$

Then, appropriate stress and strain models were developed to describe the behaviour of root-reinforced silty clay when subjected to external forces and/or fluid flow. Applying the Newton's second law and the basic principles of soil mechanics, a momentum balance equation was constructed to describe the interaction between soil and fluid. Assuming: ϑ represents the bulk density, then there is:

$$\sigma_{uk,y} + \vartheta h_y = \vartheta \frac{\partial c}{\partial y} \tag{8}$$

Then the Darcy's law was used to describe the flow behaviour of fluid in porous media, and the equation was combined with the fluid continuity equation. Considering that the root system may introduce additional resistance force or channeling effect, it is necessary to add a nonlinear term in the fluid motion equation. Assuming: j represents the permeability coefficient of the fluid, then there is:

$$w_u = j\left(o - \vartheta_q z_k h_k\right) \tag{9}$$

The next step is to determine the model boundary as fixed-pressure type, fixed-flow type, or mixed type, consider the possible temperature or chemical actions, and construct suitable boundary condition equation according to actual situation and the requirement of the model. In this paper, the boundary conditions in seepage calculation were summarized into four types. Assuming: w_b represents flow speed in the normal direction outside of the boundary, g represents the seepage coefficient, o represents the boundary pore water pressure, then there is:

$$w_b = g\left(o - o_r\right) \tag{10}$$

From the four aspects of study mentioned above, this paper created a comprehensive theoretical framework for understanding the behaviour of root-reinforced silty clay under seepage-stress coupling conditions and revealing its intrinsic mechanisms under the influence of complex environmental factors. Next, the temperature-stress coupling was calculated and temperature was added as an extra field variable based on the existing porous medium model. Employing the thermoelasticity theory, the thermal stress and thermal deformation caused by temperature changes were taken into account and added in the model. At last, the temperature-stress coupling was simulated numerically to figure out how the temperature changes affect the stress state of soil mass.

Specifically, the Fourier's law was first drawn to define the thermal conductivity and was correlated with the pore characteristics and thermal conductivity discussed above. Based on the Fourier's law, a heat transfer equation was established to describe the distribution of heat in soil mass. Assuming: Θ represents the amount of heat flowing through area S, η represents the thermal conductivity, w represents the heat flow density, S represents the area of heat transfer, then the expression is:

$$w = \frac{\Theta}{S} = -\eta \frac{dY}{dz} \tag{11}$$

Define heat within the soil unit, and consider possible phase changes or chemical reactions. Applying the principle of the conservation of heat, a complete heat conservation equation was established. Assuming: ξ^Y represents the heat capacity in per unit volume of pore medium, w^u represents the heat flow vector, $w^Y{}_c$ represents the intensity of heat source, then the heat conservation equation can be expressed as:

$$-w^Y_{u,u} + w^Y_c = \frac{\partial \varsigma^Y}{\partial y} \tag{12}$$

Both energy storage and volumetric strain can cause changes in the temperature of root-reinforced silty clay. In this paper, the heat-induced strain was defined and its interaction with mechanical strain was considered. Then, a thermal constitutive model was built to describe the response of soil mass under the action of temperature and stress. Assuming: L_{yg} and α_{yg} represent material constants, Y represents the

temperature, y represents the time, then the thermal constitutive model is given by the following formula:

$$\frac{\partial Y}{\partial y} = L_{yg}\left(\frac{\partial \varsigma^{Y}}{\partial y} - \alpha_{yg}\frac{\partial \gamma}{\partial y}\right) \tag{13}$$

In the existing thermal constitutive model, a coupling term describing the thermal-mechanical interactions was introduced further to build a new thermal constitutive model to describe the behavior of soil mass under the action of temperature and stress. Assuming: ϑ represents the average mass density of the medium, V_c represents the specific heat, then the thermal coupling constitutive equation is given by the following formula:

$$\vartheta V_c \frac{\partial Y}{\partial y} = \frac{\partial \varsigma^{Y}}{\partial y} \tag{14}$$

By combining the Fourier equilibrium equation, the heat conservation equation, and the thermal constitutive equation, a differential equation describing the heat transfer was established and solved using appropriate numerical method, as shown below:

$$\vartheta V_c \frac{\partial Y}{\partial y} - \eta Y = w_c \tag{15}$$

At last, this paper defined a strain increment term caused by temperature change, and established an equation describing the relationship between temperature change and strain increment of the root-reinforced silty clay. Assuming: β_Y represents the linear thermal expansion coefficient, then there is:

$$\Delta\gamma_{uk} = \beta_Y \Delta Y \sigma_{uk} \tag{16}$$

Through the calculation of six aspects mentioned above, we can have a comprehensive understanding of the complex response mechanism of root-reinforced silty clay under the combined effect of temperature and stress, and this knowledge could provide solid theoretical evidence for predicting soil mass in engineering applications. Further, this paper calculated the coupling of temperature-seepage, considered the influence of temperature on seepage properties (such as permeability coefficient), and updated the model parameters. After the temperature dependence had been considered, numerical simulation of temperature-seepage coupling was carried out.

Specifically, at first, a porous medium model was defined and used to describe the interactions of soil, water and root system. Then, a coupling term was introduced into the constitutive equation to capture the interaction between temperature and seepage. Assuming: ξ represents the fluid volume in per unit volume of the porous medium, α represents the volumetric expansion coefficient without drainage, then the constructed constitutive equation is:

$$\frac{\partial o}{\partial y} = L\left(\frac{\partial \varsigma}{\partial t} y - \beta\frac{\partial \gamma}{\partial y} + \alpha\frac{\partial Y}{\partial y}\right) \tag{17}$$

Assuming: β_d represents the linear thermal expansion coefficient of the fluid, b represents the porosity, then there is:

$$\alpha = 3\left[\beta_y\left(\beta - b\right) + \beta_d b\right] \tag{18}$$

Further, the basic relationship between pore pressure, soil properties (such as porosity and soil saturation), and external conditions (such as temperature and stress), was defined, with the thermal expansion or contraction of soil and water caused by temperature change and how these factors affect pore pressure taken into consideration, a mathematical equation describing the change of pore pressure with temperature was established, and its expression is:

$$\Delta o_{TH} = L\alpha\Delta Y \tag{19}$$

Through the calculation of two key aspects mentioned above, we can have a thorough understanding of the behavior of root-reinforced silty clay under temperature and seepage conditions, which lays a good theoretical foundation and can help us better manage and utilize soils of this type during actual engineering applications and environmental protection.

At last, calculation results of above three aspects were combined and analyzed to get a comprehensive and multi-perspective view showing how temperature, seepage and stress interact in the root-reinforced silty clay, and the analysis results can help us understand the intrinsic mechanism of this complex system, providing useful theoretical evidences for engineering design and environmental protection.

4. EXPERIMENTAL MATERIALS AND METHODS

4.1 Equipment and devices

Figure 1. The Model TSZ-2 full auto triaxial apparatus

Figure 2. The data collection and processing system

The triaxial apparatus is a commonly used experimental device in labs for measuring the mechanical properties of soil particles. In this study, a Model TSZ-2 full auto triaxial apparatus manufactured by the Nanjing Soil Instrument Factory was adopted in the experiment. The machine is composed of two parts: a host system, and a counter confining pressure system. The axial displacement is controlled by a stepping motor with full-range step-less speed regulation, which can generate strain and displacement precisely; and counter confining pressure is controlled by a precise hydraulic system equipped with precise digital pistons, which can apply counter confining pressure precisely while measuring the volume change and drainage. Besides the conventional unconfined stress-strain tests, and the *UU*, *CU*, *CD* and other compression shear tests, the device can also be used in stage loading, continuous loading and other consolidation tests and triaxial tests with full-automatic vibration control. Main technical data are: specimen diameter (39.1mm, 61.8mm), axial pressure (0-30 KN), shear rate (0.0024-2.4mm/min), counter confining pressure (0-2MPa), pore pressure (0-2MPa), volume change (0-50ml), two photos of the experimental devices are given by Figure 1 and Figure 2.

4.2 Test site

The test site is at Xingtai section K35+373 of Taihangshan Expressway in Hebei Province of China. The cutting section is located in a low hilly area running through the ridge line of the mountain, the ground elevation is between 244.06-258.66m, and the terrain is quite undulating. The test site is on a slope where surface runoff can be formed rapidly and discharged to lower parts of the site when raining. After some rain water infiltrates into the soil layer or fissures of bedrock formed by intense weathering, it runs and discharges towards lower parts along the bedrock surface or through the fissures, so groundwater is not easily stored in the test site, and we can say that the test site is insufficient in groundwater and its hydrogeological conditions are simple. Plants on the soil and rock slope set for the ecological restoration of the side slope are mainly mixed herbaceous plants including alfalfa (*Medicago sativa*), bermuda grass (*Cynodon dactylon*), Japanese bush clover (*Kummerowia striata*), wild mugwort (*Artemisia lavandulaefolia*), and marigold (*Tagetes erecta*), wherein the marigolds have dense branches and leaves and well-developed root systems, they usually grow in patches and can effectively intercept and alleviate soil erosion caused by rainwater, in northern regions, its effect on soil and water restoration is quite obvious. Photos of the test site and marigold samples are shown in Figure 3 and Figure 4.

Figure 3. The test site

Figure 4. Marigold sample

4.3 Specimen preparation

4.3.1 Prepare the raw root-containing soil specimens

Soil samples were taken from a ground section with gentle slope and average vegetation cover at the test site. A 1m area was selected as the area of soil sampling, and the soil mass around this area was carefully dug to a preset depth. Then, the sampled soils were cut into cubic pieces with a side length of 20cm using a wire saw and a scraper knife, then wrapped and sealed with cling film and sent to the geotechnical laboratory, where the raw root-containing soil specimens were prepared according to the specifications stipulated in the *Standard for Soil Test Method* (GB/T 50123-2019) [28] and the *Test Methods of Soils for Highway Engineering* (JTG 3430-2020) [29]. The cubic soil samples were chipped with a scraper knife and processed into standard root-containing soil specimens with a diameter of 39.1 mm and a height of 80 mm, photos of specimen preparation and the plant samples are shown in Figure 5 and Figure 6.

Figure 5. Preparation of root-containing soil specimens

Figure 6. Samples of marigolds

4.3.2 Preparation of reshaped root-containing soil specimens

As can be seen in Figure 6, main roots of marigolds distribute vertically while fibrous roots extend laterally, and the reshaped soil specimens were prepared according to the actual root system distributions. The soil specimens were test pieces made after the raw soils were subjected to shear tests, the raw soils were weighed for their total mass and then dispersed and air-dried for 2 hours until the roots can be peeled off. The preparation method was drawn from the *Standard for Soil Test Method* (GB/T 50123-2019) [28] and the *Test Methods of Soils for Highway Engineering* (JTG 3430-2020) [29], and the preparation process can be divided into seven steps:

(1) The mass of wet soil was weighed using an electronic balance with a division value of 0.01g;

(2) Soil clods were dried in an electric oven at 105°C to 110°C for 8h until the weight was constant;

(3) The dried soil samples were cooled in a desiccator to room temperature, then the dry soil mass was weighed;

(4) The soil samples were placed on a rubber plate and crushed by a soil mill into particles and then sieved (particle size of silty clay <0.075mm);

(5) According to the calculation formulas of water content and dry density, the amount of water required for reshaping the soil and the dry soil mass were calculated; based on the preset water content, a water sprayer was used to spray water on the soil samples uniformly, then the soil samples were stirred evenly, sealed, and placed in a soil container to stand for more than 24 hours before use;

(6) The prepared soil samples and plant roots were divided into 4 equal parts, after soil was filled into a split-spoon cylinder molding machine for 1/3, plant roots were added vertically into the machine according to the root content in test plan, then soil was again filled into the machine until it's full;

(7) A compactor and a demoulder were used to compact the samples and make them into cylinder-shaped specimens with a diameter of 39.1 mm and a height of 80 mm.

Triaxial *CU* tests were performed under the condition of 0.08 mm/min shear rate. Four raw soil samples were taken from each of three soil depths, some of which were root-less soils. To get the effective shear strength index of raw soils, pressure on the specimen should be kept close to the actual confining pressure of the soil mass, so in the test, the confining pressure value was set as 50kPa, 100kPa, and 200kPa. To ensure the effects of plant roots on the shear strength of soil mass at different depths, the depths and water contents were selected as: 16.7% water content at 20cm depth; 23.4% water content at 40cm depth; 28.6% water content at 60cm depth. According to the calculation of mass ratio, the root content of the reshaped root-soil composites was set to be 0%, 0.23%, 0.46%, 0.69%, 0.92% and 1.2% respectively, and the water content was set as 16.7%, 23.4% and 28.6% respectively. Parameter indexes of the silty clay samples are given in Table 1.

Table 1. Parameters of silty clay sample groups

Sample Group	Depth/cm	Water Content ω/%	Dry Density ρ_d/(g/cm^3)	Root Diameter/mm	Length of Main Root System/cm
Root content of raw soil 0%	0~20	16.7	1.58	/	/
Root content of raw soil 0.12%	0~20	16.7	1.58	4.7	11.4
Root content of raw soil 0.20%	0~20	16.7	1.58	6.1	13.2
Root content of raw soil 0.31%	0~20	16.7	1.58	6.4	14.6
Root content of raw soil 0%	20~40	23.4	1.42	/	/
Root content of raw soil 0.11%	20~40	23.4	1.42	3.7	10.6
Root content of raw soil 0.15%	20~40	23.4	1.42	3.2	9.3
Root content of raw soil 0.18%	20~40	23.4	1.42	4.3	12.9
Root content of raw soil 0%	40~60	28.6	1.33	/	/
Root content of raw soil 0.06%	40~60	28.6	1.33	2.3	5.4
Root content of raw soil 0.07%	40~60	28.6	1.33	2.6	4.5
Root content of raw soil 0.09%	40~60	28.6	1.33	1.6	6.5
Root content of reshaped soil 0%	/	16.7	1.76	/	/
Root content of reshaped soil 0.23%	/	16.7	1.76	2.7	7.2
Root content of reshaped soil 0.46%	/	16.7	1.76	4.3	6.2
Root content of reshaped soil 0.69%	/	16.7	1.76	3.2	7.8
Root content of reshaped soil 0.92%	/	16.7	1.76	6.0	6.4
Root content of reshaped soil 1.2%	/	16.7	1.76	5.7	6.6
Root content of reshaped soil 0%	/	23.4	1.58	/	/
Root content of reshaped soil 0.23%	/	23.4	1.58	2.9	7.5
Root content of reshaped soil 0.46%	/	23.4	1.58	3.2	6.9
Root content of reshaped soil 0.69%	/	23.4	1.58	3.4	6.3
Root content of reshaped soil 0.92%	/	23.4	1.58	6.8	7.7
Root content of reshaped soil 1.2%	/	23.4	1.58	5.7	7.5
Root content of reshaped soil 0%	/	28.6	1.48	/	/
Root content of reshaped soil 0.23%	/	28.6	1.48	1.5	6.4
Root content of reshaped soil 0.46%	/	28.6	1.48	4.7	6.9
Root content of reshaped soil 0.69%	/	28.6	1.48	4.7	7.5
Root content of reshaped soil 0.92%	/	28.6	1.48	5.3	7.2
Root content of reshaped soil 1.2%	/	28.6	1.48	6.3	7.7

5. EXPERIMENTAL RESULTS AND ANALYSES

Figure 7 depicts stress-strain curves for rootless soil and root-soil composites with root concentrations of 0.12%, 0.20%, and 0.31% (w: 16.7%, h: 0-20 cm). Figure 8 presents curves for rootless soil and composites with root proportions of 0.11%, 0.15%, and 0.18% (w: 23.4%, h: 20-40 cm).

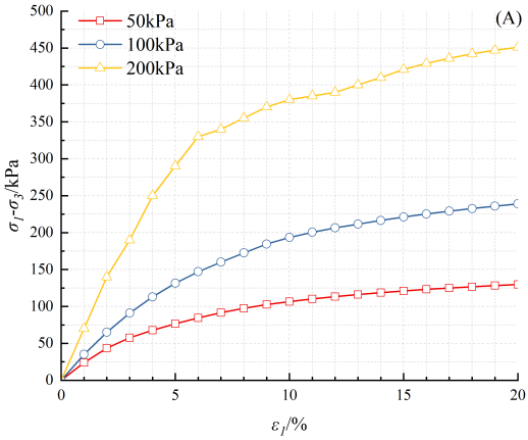

(A) rootless soil

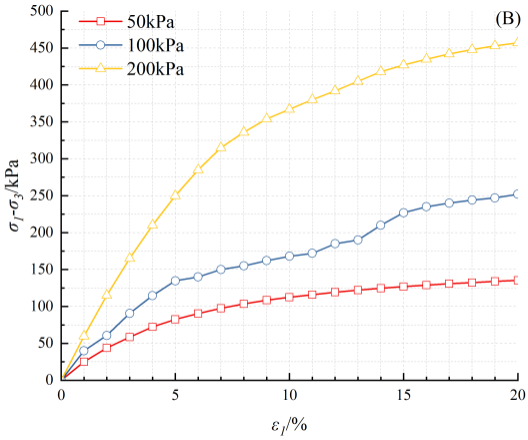

(B) 0.12% root content

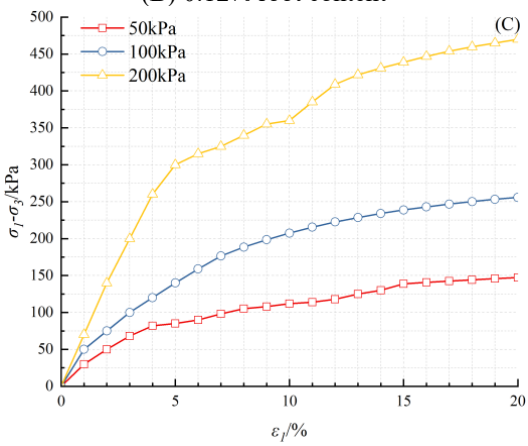

(C) 0.20% root content

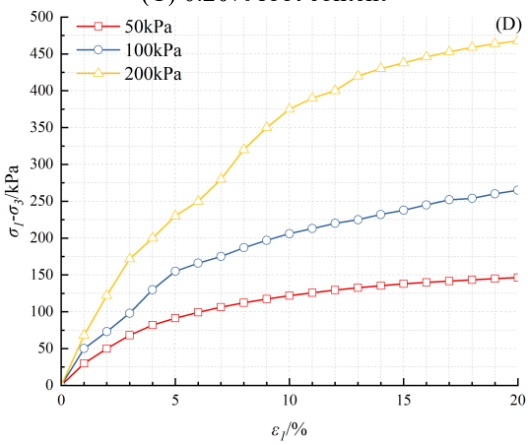

(D) 0.31% root content

Figure 7. Stress-strain curves of raw rootless soil samples and raw root-soil composite samples

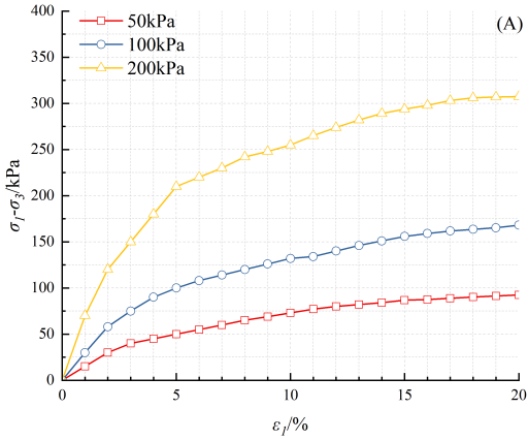

(A) rootless soil

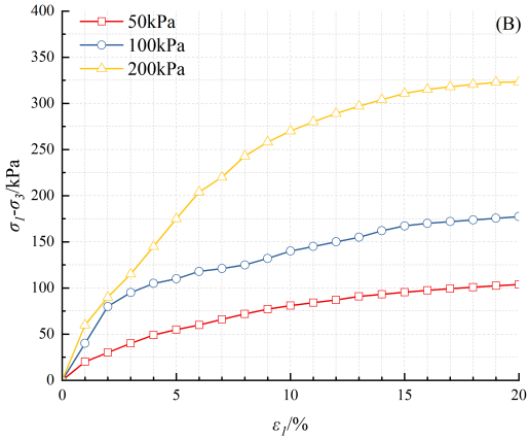

(B) 0.11% root content

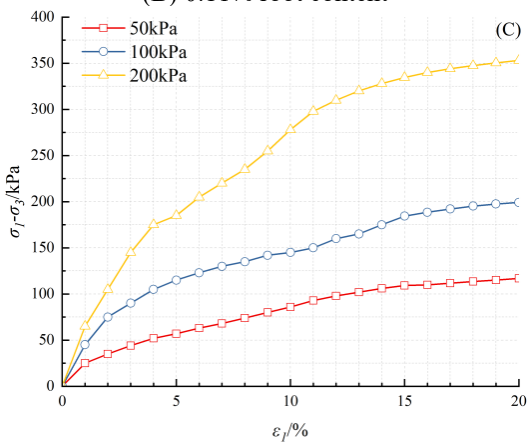

(C) 0.15% root content

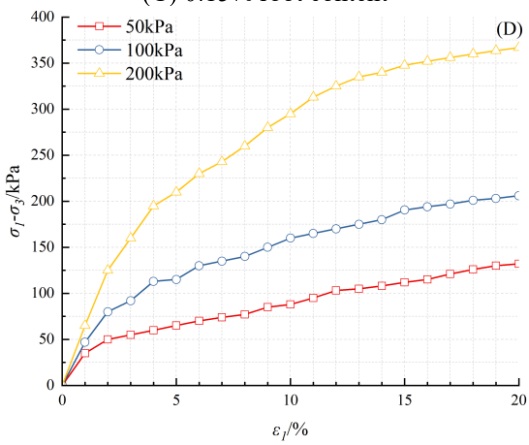

(D) 0.18% root content

Figure 8. Stress-strain curves of raw rootless soil samples and raw root-soil composite samples

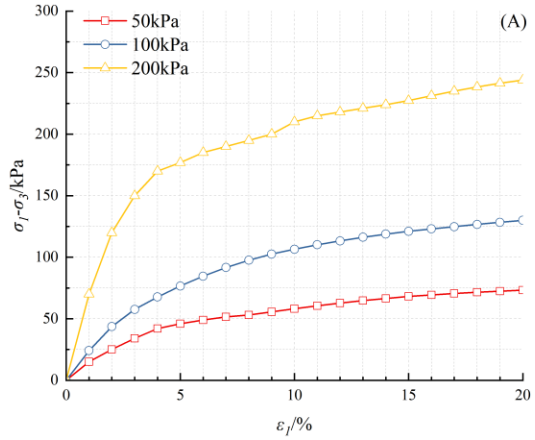

(A) rootless soil

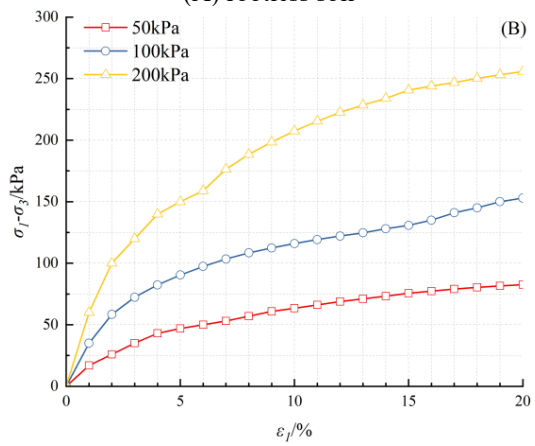

(B) 0.06% root content

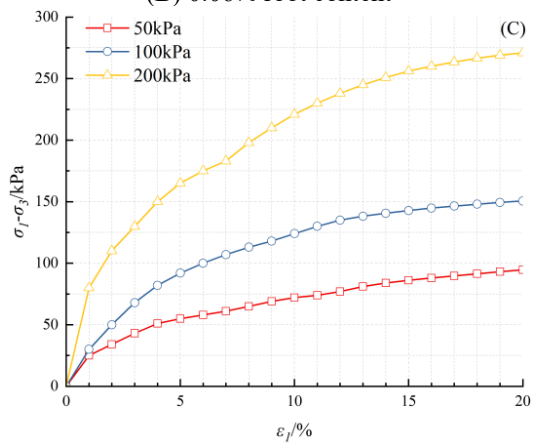

(C) 0.07% root content

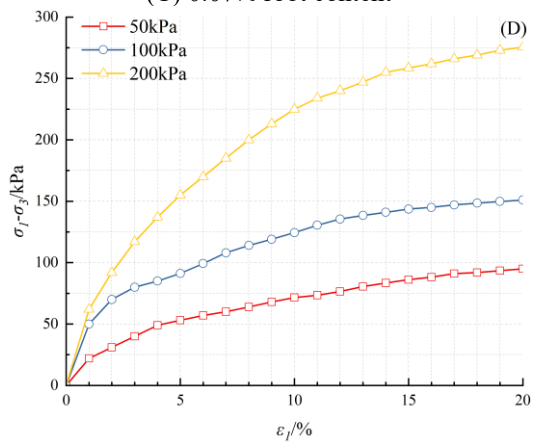

(D) 0.09% root content

Figure 9. Stress-strain curves of raw rootless soil samples and raw root-soil composite samples

The stress-strain curves of raw rootless soil samples and raw root-soil composite samples with a root content of 0.06%, 0.07%, and 0.09% (w: 28.6%, h: 40-60 cm) are shown in Figure 9.

Using the stress-strain relationships in Figures 7-9 and the Mohr-Coulomb failure criterion, shear strength envelopes are plotted in Figure 10, representing soil sample cohesion and internal friction angle. Table 2 lists the shear strength index values for raw root-soil composites.

Figures 7-9 show that the stress-strain curves for silty clay at different depths are similar for both root-soil composites and rootless soils, with four main observations:

(1) Principal stresses and axial strain both tend to increase together.

(2) Increasing the confining pressure also increases the difference between maximum and minimum principal stresses.

(3) Stress-strain curves are gentler at lower confining pressures and steeper at higher pressures.

(4) The difference between the principal stresses of raw root-soil composites increases slowly with axial strain.

Table 2 shows that cohesion increments for the root-soil composite group are between 30% and 90%, decreasing with rising water content and depth. Figure 10 indicates that the deviation of failure stress approaches a limit value at certain root contents.

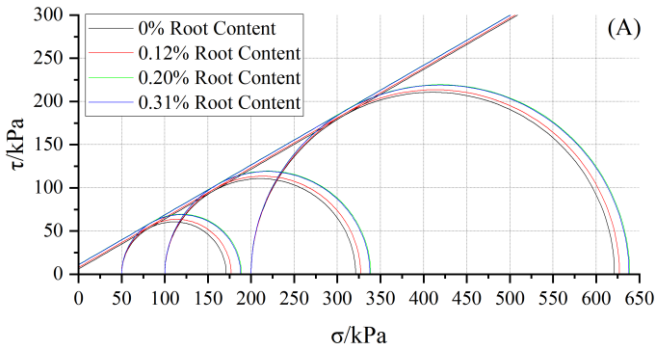

(A) w:16.7%, h:0~20cm

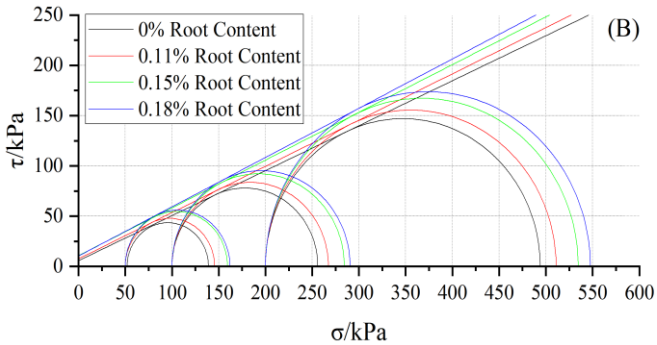

(B) w:23.4%, h:20~40cm

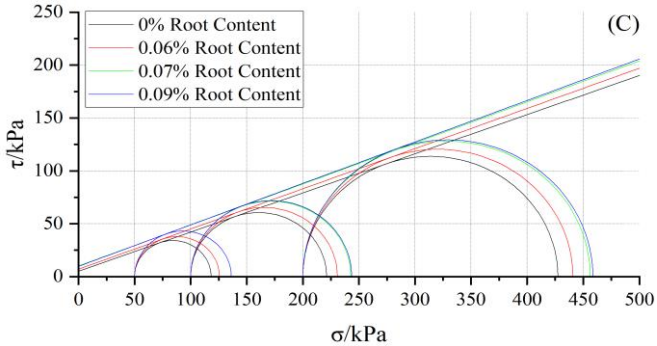

(C) w:28.6%, h:40~60cm

Figure 10. Shear strength envelopes

Table 2. Shear strength index values of raw root-soil composites

Impact Parameters	Root Content/%	Internal Friction Angle/(°)	Cohesion/kPa	Additional Cohesion of Root System/kPa
w:16.7%,*h*:0~20*cm*	0	29.2	6.1	0
	0.12	29.8	7.8	1.7
	0.20	30.2	11.2	5.1
	0.31	30.9	10.9	4.8
w:23.4%,*h*:20~40*cm*	0	24.1	5.8	0
	0.11	24.7	7.6	1.8
	0.15	25.4	10.8	5.0
	0.18	26.1	10.4	4.6
w:28.6%,*h*:40~60*cm*	0	20.3	5.2	0
	0.06	20.8	7.1	1.9
	0.07	21.2	10.1	3.0
	0.09	21.4	9.8	2.7

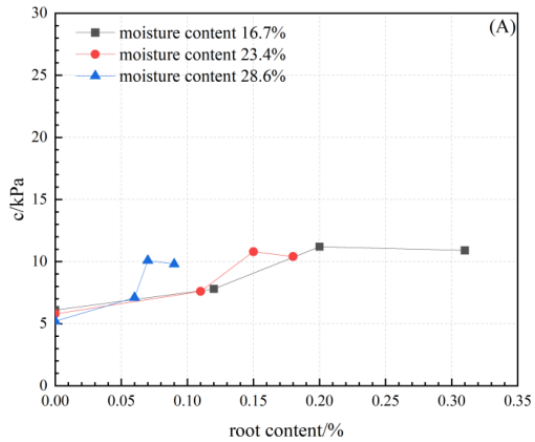

(A) Cohesion

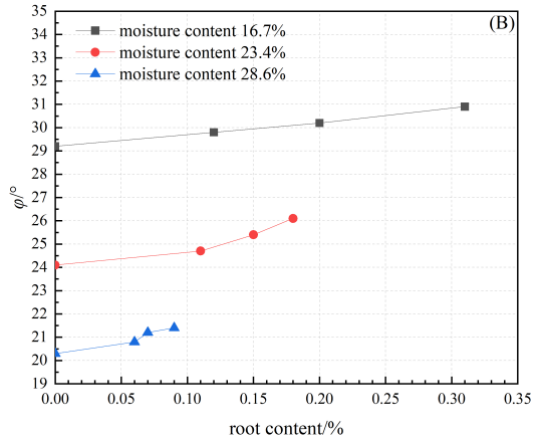

(B) Angle of internal friction

Figure 11. Relationships between cohesion, angle of internal friction, and root content under different water content values

The relationships between root content and cohesion, and between root content and the angle of internal friction of raw soils under different water content values are shown in Figure 11. Curves with a degree of fit greater than 0.8 are usually considered well-fitted in engineering practice, so the results suggest that the root content of the raw root-soil composites changed linearly with cohesion and the angle of internal friction, as the root content grew, the cohesion increased first and decreased later, while the angle of internal friction increased gently; as the water content grew, both cohesion and the angle of internal friction decreased gradually.

Under different root and water content values, the relationships with cohesion and the angle of internal friction of the raw root-containing soils are shown in Figure 12. The degree of fit of the correlation between cohesion, angle of internal friction, and root and water content is R^2>0.83 and R^2>0.99, respectively, the fitting results are of high level of confidence. With the increase of root content, the cohesion showed sharp increase and slow decrease, while the angle of internal friction showed a gentle increase; under a same root content, with the increase of water content, the angle of internal friction decreased significantly. For the cohesion, the root content plays a main role; while for the angle of internal friction, the water content is a major factor.

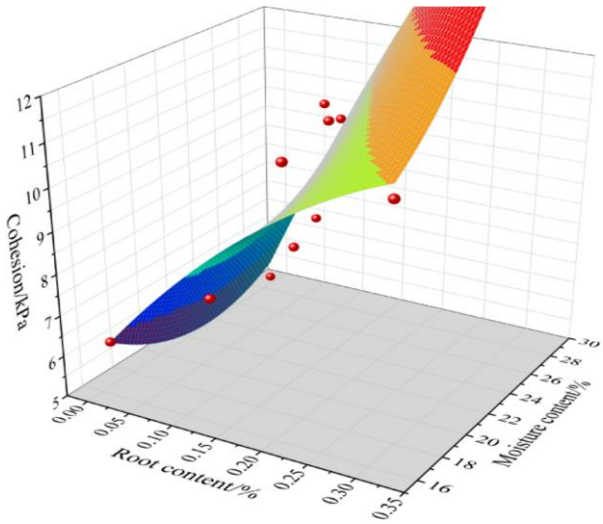

(A) Cohesion

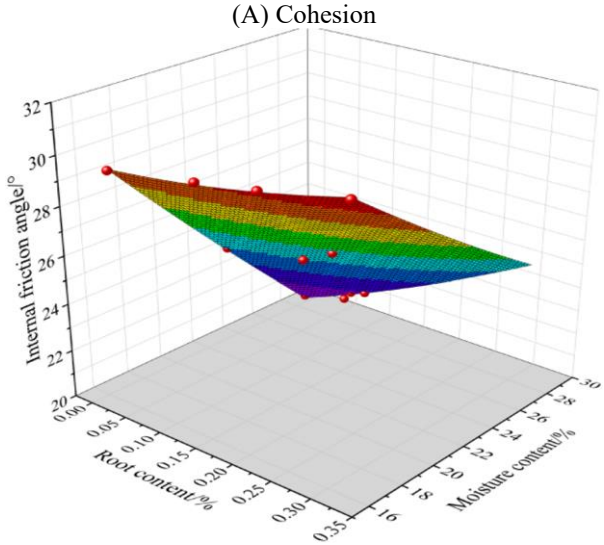

(B) Angle of internal friction

Figure 12. Relationships between cohesion, angle of internal friction, and root and water content

Table 3. Fitting results of shear strength index of raw root-soil composites

X	$X= Z_0+aG+bw+cG^2+dw^2+eGw$						R^2
	Z_0	a	b	c	d	e	
c	17.584	-5.135	-1.066	-27.182	0.023	1.802	0.836
φ	43.901	-11.233	-0.944	9.345	0.004	0.831	0.998

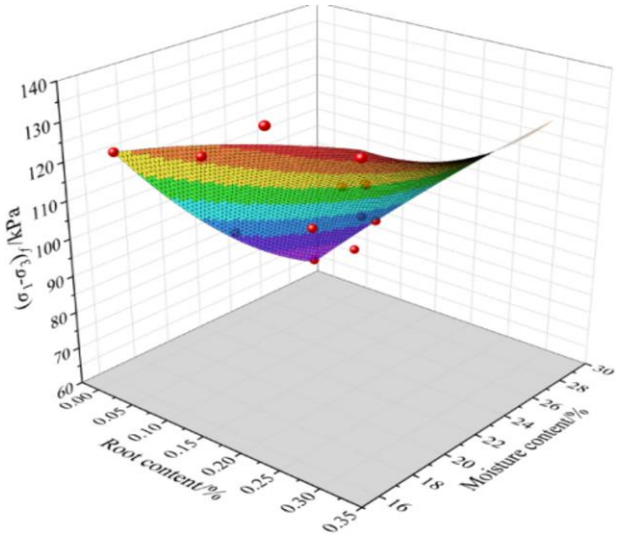

(A) σ3:50kPa

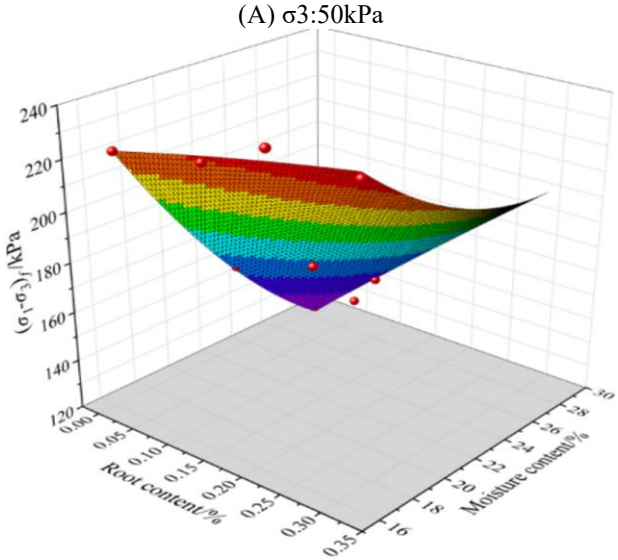

(B) σ3:100kPa

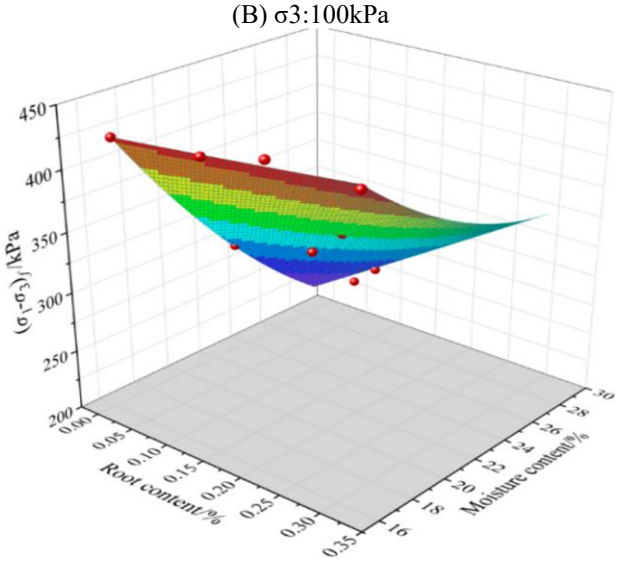

(C) σ3:200kPa

Figure 13. Relationships between deviation of failure stress and root and water content

Under different conditions of confining pressure, the relationships between the deviation of failure stress of root-containing soils and the root and water content are shown in Figure 13 and Table 3. The degree of fit of the correlation between the deviation of failure stress of root-containing soils and the root and water content is R^2>0.96, and the fitting results are of a high level of confidence. With the increase of confining pressure, the degree of fit was close to 1, indicating that the increment of stress deviation caused by root content and the decrement of stress deviation caused by water content had offset each other.

Under a same water content (about 15.2%), the thermal conductivity of root-reinforced silty clay was observed as the dry density grew from 1.5 to 1.7. As can be seen from Table 4, the average thermal conductivity increased from 1.284 to 1.426 as the dry density grew from 1.5 to 1.7. Within each group, the variations of thermal conductivity were relatively small, indicating that under a same dry density, the thermal conductivity was stable. When the dry density increased from 1.5 to 1.7, the average thermal conductivity also showed an upward trend, thus it can be concluded that under a same water content, the dry density has a significant effect on the thermal conductivity of root-reinforced silty clay. Specifically, the thermal conductivity increased as the dry density grew. Within test groups with a same dry density, the variations of thermal conductivity were relatively small, indicating that under such conditions, the thermal conductivity of root-reinforced silty clay was relatively stable.

Data in Table 5 show that when the dry density grew from 1.3 to 1.5, the logarithmic value of thermal conductivity increased from 0.0678 to 0.1328. In some cases, the thermal conductivity predicted by the *Kersten* model was close to the measurement (such as No. 3), while in other cases, there were large differences (such as No. 4 and No. 5). When the dry density grew from 1.3 to 1.5, the measured value of thermal conductivity increased from 1.248 to 1.326, so it can be concluded that there is a positive correlation between dry density and the logarithmic value of thermal conductivity, that is, when dry density increases, the coefficient of thermal conductivity increases as well, and this is consistent with the previous analysis results. The prediction results of the *Kersten* model are close to actually measured data in some cases but not always accurate. This implies that more research is needed to improve or calibrate the *Kersten* model so as to adapt to the root-reinforced silty clay.

According to Figure 14, when pore pressure increased from 2 MPa to 4 MPa, permeability increased at all temperatures. In case of low temperatures (5 and 7 degrees Celsius), the permeability was higher; while at high temperatures (9, 11, and 13 degrees Celsius), the permeability decreased gradually. High pore pressure and high temperature seem to have a multiplicative effect on permeability. For example, under the condition of 4 MPa and 5 degrees, the permeability was 135, which was much higher than other conditions. So it can be concluded that there is a positive correlation between pore pressure and permeability. This is because the increase in pore pressure can lead to a denser soil structure, thereby increasing

the resistance of the water flow. The relationship between temperature and permeability is complex, but the general trend is that as temperature increases, permeability decreases. Under high pore pressure and low temperature conditions, permeability increases significantly, which is due to the different pore structures and flow properties of soil under these conditions.

Table 4. Test results of thermal conductivity of root-reinforced silty clay samples under a same water content and different dry densities

Group by Dry Density	Dry Density	Water Content	Thermal Conductivity	Average Value of Thermal Conductivity
	1.5	15.2	1.265	
1	1.5	15.1	1.238	1.284
	1.5	15.3	1.248	
	1.55	14.8	1.325	
2	1.55	15.3	1.348	1.358
	1.55	15.4	1.322	
	1.6	15.2	1.328	
3	1.6	15.1	1.489	1.345
	1.6	15.2	1.348	
	1.65	15.1	1.478	
4	1.65	15.2	1.462	1.428
	1.65	15.4	1.413	
	1.7	15.2	1.425	
5	1.7	15.2	1.489	1.426
	1.7	15.3	1.426	

Table 5. Relationship between dry density of root-reinforced silty clay and the logarithmic value of thermal conductivity

No.	Dry Density	Logarithmic Value of Thermal Conductivity	Measured Value of Thermal Conductivity	Thermal Conductivity Predicted by the *Kersten* Model
1	1.3	0.0678	1.248	1.024
2	1.35	0.0952	1.304	1.087
3	1.4	0.1245	1.215	1.215
4	1.45	0.1329	1.458	1.136
5	1.5	0.1328	1.326	1.268

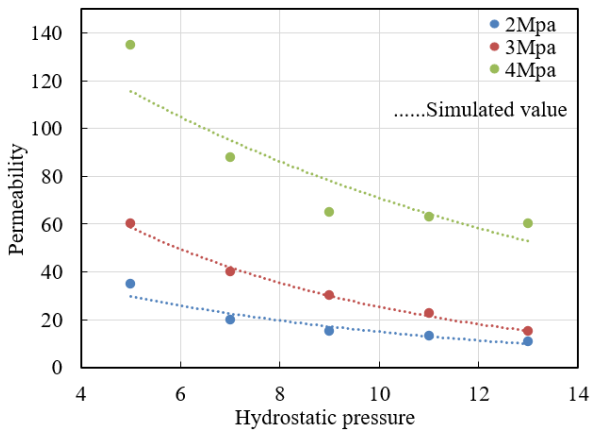

Figure 14. Permeability versus hydrostatic pressure of root-reinforced silty clay specimens at different temperatures

According to Table 6, when dry density increased from 1.3 to 1.5, the actually measured value of thermal conductivity increased as well. There isn't an obvious direct correlation between the fractal dimension of particle distribution (an index describing the complexity or diversity of particle distribution) and the measured thermal conductivity. The values of Prediction 1 are always lower than the measured thermal conductivity, while the values of Prediction 2 are closer to the measured values, thus it can be concluded that there is a positive correlation between dry density and the measured thermal conductivity. This is in line with our previous research and the basics of soil physics. The relationship between the fractal dimension of particle distribution and thermal conductivity is not obvious, which indicates that further research is needed to understand the subtle and complex interactions between the two. In terms of thermal conductivity prediction, the values of Prediction 2 are more accurate, indicating that when the thermal conductivity properties of root-reinforced silty clay are involved, the model or methodology based on which the values of Prediction 2 were attained is more reliable.

Table 6. Comparison of measured thermal conductivity and predicted fractal dimension of particle distribution of root-reinforced silty clay specimens

Dry Density	Fractal Dimension of Particle Distribution	Measured Thermal Conductivity	Prediction 1	Prediction 2
1.3	1.8512	1.2015	1.002	1.254
1.35	1.8526	1.1258	1.087	1.125
1.4	1.8633	1.1563	1.235	1.163
1.45	1.8541	1.2369	1.158	1.1254
1.5	1.8971	1.2547	1.236	1.1239

Table 7. Comparison of measured thermal conductivity and predicted fractal dimension of pore diameter distribution of root-reinforced silty clay specimens

Dry Density	Fractal Dimension of Pore Diameter Distribution	Measured Thermal Conductivity	Prediction 1	Prediction 2
1.3	1.215	1.274	1.002	1.252
1.35	1.158	1.324	1.088	1.177
1.4	1.3297	1.328	1.125	1.199
1.45	1.652	1.288	1.299	1.246
1.5	1.4238	1.245	1.234	1.286

Data in Table 7 show that when dry density increased from 1.3 to 1.5, the measured thermal conductivity didn't change much but fluctuated a little. There isn't an obviously consistent pattern between the fractal dimension of pore diameter distribution (an index describing pore size and distribution) and the measured thermal conductivity. Values of Prediction 1 and Prediction 2 are all close to the measured thermal conductivity, and the values of Prediction 2 are closer, so it can be concluded that the relationship between dry density and measured thermal conductivity is quite complicated, which is caused by multiple factors, including soil pore structure and particle distribution, etc. There isn't an obvious consistency between the fractal dimension of pore diameter distribution and the thermal conductivity, which implies that there are other potential influence factors or interactions between these two parameters. Values of Prediction 2 are closer to the measured thermal conductivity, suggesting that the model or methodology based on which the values of Prediction 2 were attained is more reliable.

According to Figure 15, in case that the pore pressure was 2Mpa, 3Mpa and 4Mpa, respectively, with the increase of volumetric strain (0.06, 0.12, 0.19), the permeability decreased significantly. This is because the increase of soil density caused by volumetric strain had reduced seepage channels. Under various pore pressure values, volumetric strain and permeability were always negatively correlated, especially in case of increased pore pressure, under a same volumetric strain, the permeability increased accordingly as well. When pore pressure increased from 2 MPa to 4 MPa, the permeability increased correspondingly, implying an approximately linear relationship between the two. Therefore, it can be concluded that both pore pressure and volumetric strain are important factors affecting the permeability of root-reinforced silty clay. As the volumetric strain increased, the permeability decreased, this is because the increase of the compactness of soil had changed the pore structure and reduced seepage channels. The increase of pore pressure can significantly increase permeability, and this is related to the mechanical properties and pore structure of the soil.

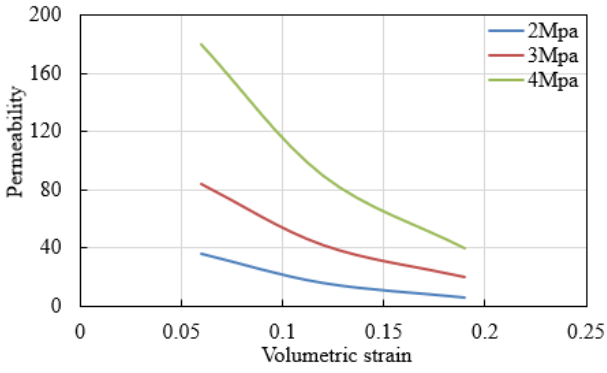

Figure 15. Permeability versus volumetric strain of root-reinforced silty clay specimens at different temperature

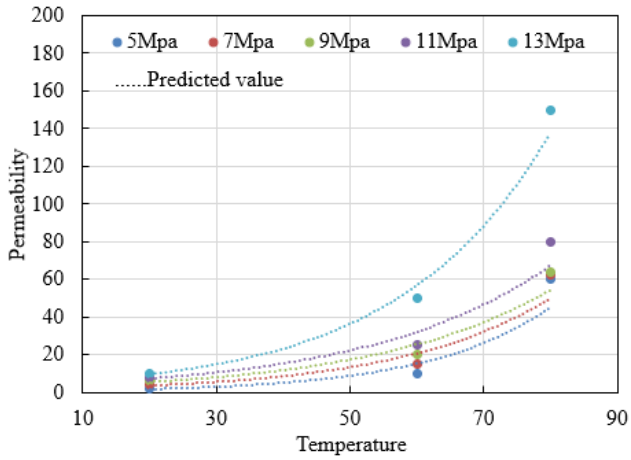

Figure 16. Permeability versus temperature of root-reinforced silty clay specimens at different pore pressures

According to Figure 16, under different confining pressures (5Mpa, 7Mpa, 9Mpa, 11Mpa, 13Mpa), with the rise of temperature (20, 60, 80 degrees), the permeability increased significantly, this is because the temperature rise had reduced soil viscosity, thereby increasing pores and seepage channels. Under high confining pressures and a same temperature, the permeability increased accordingly, but such increase was not linear, especially under a confining pressure of 13 MPa, the permeability increased significantly. When the confining pressure increased from 5Mpa to 13Mpa, the permeability also increased at all temperatures, but the increment at 80 degrees was the most significant. Thus it can be concluded that confining pressure and temperature are both key factors affecting the permeability of root-reinforced silty clay. Temperature rise usually increases permeability, and this is related to the mechanical properties and viscosity of the soil. Under high confining pressures, the increase of permeability is more obvious, especially at high temperatures. This is because the joint effects of high confining pressure and high temperature had caused changes in soil structure, thereby increasing the permeability.

6. CONCLUSION

This paper used two core contents to fill in these research gaps: first, based on experiment and numerical simulation, it gave a detailed analysis on the relationship between pore characteristics and thermal conductivity of root-reinforced silty clay, as well as its impact on shear strength; second, it used a temperature-seepage-stress coupling model to give a comprehensively study on the thermal stress behaviour of root-reinforced silty clay. Also, the equilibrium equation of saturated pore medium, the momentum balance equation in fluid-solid coupling calculations, the equation of fluid motion, and the boundary conditions of seepage were investigated. The

Fourier equilibrium equations, the heat conservation equation, the thermal constitutive equation, and constitutive equation of thermodynamic coupling, and other aspects were explored. This study took the composites of marigold roots and soils as the subject to measure and evaluate the effect of the root system of herbaceous Asteraceae plants in Taihang Mountain on enhancing erosion resistance, soil consolidation, and shear performance of soil mass. Then it discussed the constitutive equation and the temperature-induced pore pressure changes, collected a few groups of measured data under different dry densities and water contents, and compared them with the prediction results of the *Kersten* model and other models.

Experimental results show that the difference between the maximum and minimum principal stresses of the raw root-soil composites and the axial strain didn't vary linearly but there's a tendency for the two to increase with each other; when the axial strain was constant and the confining pressure increased from 50 kPa to 200 kPa, the difference between the maximum and minimum principal stresses increased accordingly; when the applied confining pressure was smaller, the stress-strain curves tended to be gentle, and vice versa; compared with the raw root-less soil samples, for the raw root-soil composites, the increment of the difference between the maximum and minimum principal stresses showed a slow increasing trend as the axial strain increased. Under a same water content but different dry densities, the thermal conductivity of root-reinforced silty clay exhibited some changes, and there's a certain relationship between dry density and the logarithmic value of thermal conductivity. In terms of fractal dimensions of particle distribution and pore diameter distribution, the predicted thermal conductivity was basically consistent with the measured value. Under different temperatures and pore pressures, the relationship between permeability and hydrostatic pressure showed nonlinearity. Both volumetric strain and temperature affect permeability, especially at high temperatures and high pore pressure conditions. These results and conclusions are valuable for civil engineering and environmental sciences, especially for soil consolidation and soil amelioration projects.

REFERENCES

[1] Sadiq, A., Fattah, M.Y., Aswad, M.F. (2023). Enhancement of the acid resistance of silty clay using nano-magnesium oxide. Materials, 16(14): 5035. https://doi.org/10.3390/ma16145035

[2] Pan, J.J., Wang, B., Wang, Q., Ling, X.Z., Fang, R.C., Liu, J.Q., Wang, Z.H. (2023). An adhesion–ploughing friction model of the interface between concrete and silty clay. Construction and Building Materials, 376: 131039. https://doi.org/10.1016/j.conbuildmat.2023.131039

[3] Liu, J.W., Zhang, Y.X., Yuan, M.Q., Zhao, Y.D., Yang, J.S. (2022). Determining the cause of tunnel damages during tunneling in silty clay. Engineering Failure Analysis, 137: 106156. https://doi.org/10.1016/j.engfailanal.2022.106156

[4] Yang, J.C., Xia, Y.Y., Chen, W.D., Zhang, L., Li, L.H. (2023). Shear behavior of silty clay-concrete interface based on large-scale direct shear test. International Journal of Geomechanics, 23(7): 04023084. https://doi.org/10.1061/IJGNAI.GMENG-8285

[5] Xin, Q.M., Yang, T.H., She, X.K., Gao, Y., Cao, Y. (2022). Experimental and modeling investigation of thermal conductivity of Shenyang silty clay under unfrozen and frozen states by Hot Disk method. International Communications in Heat and Mass Transfer, 132: 105882. https://doi.org/10.1016/j.icheatmasstransfer.2022.105882

[6] Ji, Y.D., Zhu, K.P., Lyu, C., Wang, S.D., Ning, D.Y., Fan, J., Shi, L. (2021). Semiempirical correlation between p-wave velocity and thermal conductivity of frozen silty clay soil. Shock and Vibration, 2021: 5533696. https://doi.org/10.1155/2021/5533696

[7] Liu, X., Cai, G., Liu, L., Liu, S., Dai, J. (2019). Thermal conductivity and prediction model of mucky silty clay in Nanjing floodplain. Dongnan Daxue Xuebao (Ziran Kexue Ban)/Journal of Southeast University (Natural Science Edition), 49(5): 989-995.

[8] Liu, X.Y., Cai, G.J., Congress, S.S.C., Liu, L.L., Liu, S.Y. (2020). Investigation of thermal conductivity and prediction model of mucky silty clay. Journal of Materials in Civil Engineering, 32(8): 04020221. https://doi.org/10.1061/(ASCE)MT.1943-5533.0003294

[9] Li, Q.L., Wei, H.B., Zhang, Y.P., Han, L.L., Han, S.Y., Ding, N. (2020). The variations on thermal conductivity and structures of silty clay modified by waste fly ash and oil shale ash after freeze–thaw cycles. Construction and Building Materials, 260: 119954. https://doi.org/10.1016/j.conbuildmat.2020.119954

[10] Sun, Q., Lyu, C., Zhang, W.Q. (2020). The relationship between thermal conductivity and electrical resistivity of silty clay soil in the temperature range −20°C to 10°C. Heat and Mass Transfer, 56(6): 2007-2013. https://doi.org/10.1007/s00231-020-02813-0

[11] Sun, Q., Lü, C. (2019). Semiempirical correlation between thermal conductivity and electrical resistivity for silt and silty clay soils. Geophysics, 84(3): MR99-MR105. https://doi.org/10.1190/geo2018-0549.1

[12] Zhang, M.Y., Lu, J.G., Lai, Y.M., Zhang, X.Y. (2018). Variation of the thermal conductivity of a silty clay during a freezing-thawing process. International Journal of Heat and Mass Transfer, 124: 1059-1067. https://doi.org/10.1016/j.ijheatmasstransfer.2018.02.118

[13] Xu, J., Zhu, H., Yan, Z. (2012). Experimental studies on coefficient of thermal conductivity of silty clay. Yantu Gongcheng Xuebao/Chinese Journal of Geotechnical Engineering, 34(11): 2108-2113.

[14] Chen, B., Xu, Z., Yao, C., Zhang, H. (2012). Thermal conductivity of Shanghai (5)1 silty clay. Tongji Daxue Xuebao/Journal of Tongji University, 40(6): 843-848. https://doi.org/ 10.3969/j.issn.0253-374x.2012.06.007

[15] Evert, R.F. (2006). Esau's plant anatomy: meristems, cells, and tissues of the plant body: their structure, function, and development. John Wiley & Sons.

[16] Tan, X.Q., Huang, Y.W., Xiong, D.W., Lv, K., Chen, F.Q. (2020). The effect of Elymus nutans sowing density on soil reinforcement and slope stabilization properties of vegetation–concrete structures. Scientific Reports, 10(1): 20462. http://doi.org/10.1038/s41598-020-77407-1

[17] Zhou, Y.Y., Wang, X.M. (2019). Mesomechanics characteristics of soil reinforcement by plant roots. Bulletin of Engineering Geology and the Environment, 78: 3719-3728. https://doi.org/10.1007/s10064-018-1370-y

[18] Ma, Q., Wu, N.Z., Xiao, H.L., Li, Z., Li, W.T. (2021). Effect of Bermuda grass root on mechanical properties of soil under dry–wet cycles. Bulletin of Engineering Geology and the Environment, 80: 7083-7097. https://doi.org/10.1007/s10064-021-02369-1
[19] Schwarz, M., Lehmann, P., Or, D. (2010). Quantifying lateral root reinforcement in steep slopes–from a bundle of roots to tree stands. Earth Surface Processes and Landforms: The Journal of the British Geomorphological Research Group, 35(3): 354-367. https://doi.org/10.1002/esp.1927
[20] Foresta, V., Capobianco, V., Cascini, L. (2020). Influence of grass roots on shear strength of pyroclastic soils. Canadian Geotechnical Journal, 57(9): 1320-1334. https://doi.org/10.1139/cgj-2019-0142
[21] Cui, H.Z., Jin, Z.Y., Bao, X.H., Tang, W.C., Dong, B.Q. (2018). Effect of carbon fiber and nanosilica on shear properties of silty soil and the mechanisms. Construction and Building Materials, 189: 286-295. https://doi.org/10.1016/j.conbuildmat.2018.08.181
[22] Mei, L., Dong, X., Yang, S.Y., Deng, J. (2022). Experimental study on mechanical properties of cement-solidified remolded soil reinforces by polyvinyl alcohol fiber. Advances in Materials Science and Engineering, 2022: 5169404. https://doi.org/10.1155/2022/5169404
[23] Huang, F.K., Tsai, C.C., Ge, L., Lu, C.W., Chi, C.C. (2022). Strength variations due to re-liquefaction-indication from cyclic tests on undisturbed and remold samples of a liquefaction-recurring site. Bulletin of Engineering Geology and the Environment, 81(3): 117. https://doi.org/10.1007/s10064-022-02621-2
[24] Ahmad, W., Uchimura, T. (2023). The effect of moisture content at compaction and grain size distribution on the shear strength of unsaturated soils. Sustainability, 15(6): 5123. https://doi.org/10.3390/su15065123
[25] Lian, B.Q., Peng, J.B., Wang, X., Huang, Q.B. (2020). Moisture content effect on the ring shear characteristics of slip zone loess at high shearing rates. Bulletin of Engineering Geology and the Environment, 79: 999-1008. https://doi.org/10.1007/s10064-019-01597-w
[26] Fan, C.C., Lu, J.Z., Chen, H.H. (2021). The pullout resistance of plant roots in the field at different soil water conditions and root geometries. Catena, 207: 105593. https://doi.org/10.1016/j.catena.2021.105593
[27] Jiao, Z., Wang, D.J., Xie, H., Zhang, J.S., Guo, L.H. (2010). Experimental analysis of shear strength of undisturbed soil in leucaena forest in Jiangjia Ravine, Yunnan, China. Journal of Mountain Science, 7: 386-395. https://doi.org/10.1007/s11629-010-2053-8
[28] GB/T50123-2019 (2019). Standard for soil test methods. National Standard of the People's Republic of China, Beijing, China.
[29] JTG 3430-2020 (2020). Test method of soils for highway engineering. Industry Standards of the People's Republic of China, Beijing, China.